


## Physical properties of $\text{YbFe}_5\text{P}_3$ with a quasi-one-dimensional crystal structure

T. Asaba<sup>1</sup>, S. Lee<sup>1</sup>, S. Seo<sup>1</sup>, K. E. Avers<sup>1,2</sup>, S. M. Thomas<sup>1</sup>, R. Movshovich<sup>1</sup>,  
J. D. Thompson<sup>1</sup>, P. F. S. Rosa<sup>1</sup>, E. D. Bauer<sup>1</sup> and F. Ronning<sup>3</sup>

<sup>1</sup>*MPA-Q, Los Alamos National Laboratory, Los Alamos, New Mexico 87545, USA*

<sup>2</sup>*Department of Physics and Astronomy, Northwestern University, Evanston, Illinois 60208, USA*

<sup>3</sup>*Institute for Materials Science, Los Alamos National Laboratory, Los Alamos, New Mexico 87545, USA*

 (Received 19 July 2021; revised 12 October 2021; accepted 12 October 2021; published 22 November 2021)

We report basic physical properties of the quasi-one-dimensional heavy-fermion compound  $\text{YbFe}_5\text{P}_3$ . Its magnetic susceptibility follows a modified Curie-Weiss behavior at high temperatures with a Weiss temperature between  $-5$  and  $-21$  K depending on the direction of the applied magnetic field. Our single crystals of  $\text{YbFe}_5\text{P}_3$  are good metals with a room-temperature resistivity of  $\sim 140 \mu\Omega \text{ cm}$  and a residual resistivity of less than  $2 \mu\Omega \text{ cm}$ . Below  $\sim 2$  K the resistivity reflects the presence of strong quantum fluctuations, which is supported by specific heat measurements that show a similar strong enhancement in  $C/T$  at low temperatures reaching  $1.5 \text{ J/mol K}^2$  below  $T = 0.5$  K. No magnetic ordering is observed down to 80 mK. Magnetic fields up to 8 T rapidly suppress the magnetic fluctuations, while resistivity measurements under pressures up to 2.54 GPa indicate the enhancement of quantum fluctuations, although still no order is observed down to 0.3 K. Density functional theory calculations suggest the presence of electronically quasi-one-dimensional (1D) Fermi surface sheets together with three-dimensional electronic pockets. We suggest that the quasi-1D nature of this compound leads to an extended regime of large quantum fluctuations within the paramagnetic state prior to reaching a magnetic instability.

DOI: [10.1103/PhysRevB.104.195140](https://doi.org/10.1103/PhysRevB.104.195140)

### I. INTRODUCTION

Understanding the strange metal behavior in the vicinity of a quantum critical point (QCP) has been a long-standing mystery for many systems including high- $T_c$  superconductors [1–4]. For  $f$ -electron-based heavy-fermion metals, the Doniach diagram provides a useful starting point to describe the competition between the Ruderman-Kittel-Kasuya-Yosida (RKKY) interaction, which promotes long-range magnetic order, and the Kondo interaction, which acts to screen the magnetic  $f$  moments by the conduction electrons  $c$  [5]. Both interactions depend on the  $f$ - $c$  exchange coupling  $J$ , though with different functional forms, that can be tuned by a non-thermal control parameter, such as pressure or magnetic field. At a critical value of  $J$ , the competition of these interactions leads to a zero-temperature magnetic/nonmagnetic boundary where quantum fluctuations dominate physical properties. More recently, the Doniach diagram has been extended to include the strength of quantum fluctuations as an independent means to suppress magnetic order [6–8]. This “global” phase diagram possesses a rich variety of quantum phase transitions. An interesting proposal of this phase diagram is the possibility to find a state of matter in which the  $f$  electron undergoes a localization-delocalization transition in the absence of magnetic order, which has been suggested to occur in various frustrated  $f$ -electron systems [9–12].

Magnetic frustration and reduced dimensionality are known routes to increase the strength of quantum fluctuations. Here we focus on exploiting reduced dimensionality by con-

sidering a magnetically quasi-one-dimensional (1D) system that may possess a paramagnetic ground state wherein the  $f$  electron remains localized. Such quasi-1D magnetic systems should also be more tractable theoretically. In addition to reduced dimensionality, a clean system is strongly desired. This is because one of the significant predictions of the global phase diagram is that the size of the Fermi surface changes across the QCP. Fermiology, therefore, is an important tool to probe the phase diagram. The small energy scales in heavy-fermion compounds present a drawback for angle-resolved photoemission spectroscopy (ARPES). A very clean system exhibiting a high mobility is required to observe quantum oscillations. Such a system in the vicinity of an instability could be driven towards a QCP with a clean tuning parameter, e.g., hydrostatic pressure.

There are limited examples, however, that meet all the conditions above, and experimental studies on quasi-1D compounds with quantum phase transitions have been sparse. The most prominent examples of quasi-1D systems that have a QCP are  $\text{YbNi}_4\text{P}_2$  [13,14] and  $\text{CeRh}_6\text{Ge}_4$  [15,16], both of which possess a ferromagnetic QCP.  $\text{Yb}_2\text{Pt}_2\text{Pb}$  and  $\text{Yb}_2\text{Fe}_{12}\text{P}_7$  are two additional systems that show good evidence for quasi-1D magnetic behavior and non-Fermi-liquid behavior under applied fields [17–19]. Both order antiferromagnetically, however, at 2.0 and 0.9 K, respectively. If negative chemical pressure could be applied, it would be interesting to drive these systems through their respective quantum phase transitions.

In this paper, we report that  $\text{YbFe}_5\text{P}_3$  likely satisfies the above conditions. It is structurally quasi-one-dimensional. It is a clean system with high residual resistivity ratio (RRR), and we find evidence of strong quantum fluctuations, which suggests close proximity to a quantum phase transition.

## II. METHODS

Magnetic properties are measured in a Quantum Design Magnetic Properties Measurement System (MPMS). Specific heat measurements are carried out in an Oxford dilution fridge and a Quantum Design Physical Property Measurement System (PPMS) using short and long heat pulse methods, respectively. Transport properties are measured in a PPMS with a four-wire measurement using a digital resistance bridge with a typical excitation current of 100–330  $\mu\text{A}$  and current frequency of 13 Hz. For pressure-dependent measurements, samples are sealed in a hybrid Be-Cu/NiCrAl clamp-type cell with Daphne oil 7373 as the pressure-transmitting medium. The applied pressures were calibrated by the superconducting  $T_c$  of a Pb sample. Density functional theory (DFT) calculations are performed using the generalized gradient approximation with the Perdew-Burke-Ernzerhof (PBE) functional [20] as implemented in the WIEN2K package [21]. Spin-orbit coupling is included in a second variational manner.

## III. SYNTHESIS AND CRYSTAL STRUCTURE

Needlelike single crystals of  $\text{YbFe}_5\text{P}_3$  and  $\text{LuFe}_5\text{P}_3$  were prepared using Sn and Zn flux, respectively. Single crystals of  $\text{YbFe}_5\text{P}_3$  were grown from Sn flux [22]. Starting elements were loaded in the molar ratio of Yb:Fe:P:Sn=1:2:1.5:20 into an alumina crucible and sealed in a silica ampule under vacuum. The ampule was heated to 500°C over 10 h and held at 500°C for 6 h. The temperature was then increased to 1000°C over 12 h, and held there for 24 h. Finally, the temperature was then lowered to 700°C over 100 h, at which temperature the molten Sn flux was removed using a centrifuge. Excess Sn flux on the surface of the  $\text{YbFe}_5\text{P}_3$  crystals was removed by etching in dilute hydrochloric acid.  $\text{LuFe}_5\text{P}_3$  was prepared in a similar manner using Zn flux with a molar ratio of Lu:Fe:P:Zn=1:2:1.5:30. In this case, the Lu and Fe were arc-melted together first. The temperature for the  $\text{LuFe}_5\text{P}_3$  material was raised to 700°C over 14 h and held for 6 h. The temperature was then increased to 1100°C over 10 h, held for 8 h, then decreased to 800°C over 100 h, at which temperature the molten Zn was removed.

Powder and single-crystal diffraction confirm the crystal structure of our samples.  $\text{YbFe}_5\text{P}_3$  and  $\text{LuFe}_5\text{P}_3$  belong to the  $\text{YCo}_5\text{P}_3$ -type orthorhombic structure (space group  $Pnma$ , No. 62) with the lattice parameters  $a = 1.195$  nm,  $b = 0.365$  nm, and  $c = 1.037$  nm for  $\text{YbFe}_5\text{P}_3$  and  $a = 1.21$  nm,  $b = 0.3675$  nm, and  $c = 1.046$  nm for  $\text{LuFe}_5\text{P}_3$ , which are in good agreement with a previous study [22]. The crystal structure is shown in Fig. 1. Yb atoms form chains along the  $b$  axis with an Yb-Yb distance of 0.365 nm. The second-shortest Yb-Yb bond occurs between the chains with a distance of 0.55 nm, which is 1.5 times the intrachain distance. Furthermore, the interchain magnetic interaction is expected to be frustrated as

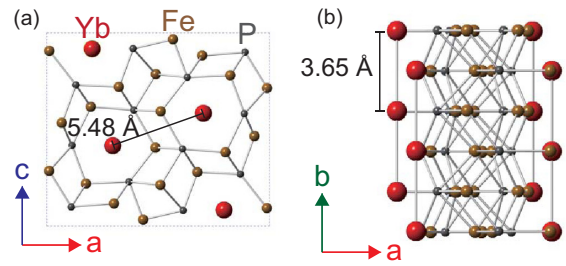


FIG. 1. Crystal structure of  $\text{YbFe}_5\text{P}_3$ . (a) Viewed down the  $b$  axis, the chain direction. The big red spheres indicate the position of Yb atoms. Medium brown spheres depict iron, and small purple spheres are for P. The dashed square indicates the unit cell. The solid lines show the nearest bonds between Fe and P atoms. (b) Viewed from the  $c$  axis. Vertical lines between Yb atoms indicate the nearest Yb-Yb distance along the chain direction, 0.365 nm.

the Yb atoms in the neighboring chain are shifted by half a unit cell along the  $b$  direction. This suggests that the magnetic interactions between Yb ions may be quasi-one-dimensional. Reflecting the crystal structure, crystals grow as needles along the  $b$  axis, with typical dimensions of  $\sim 50 \times 50 \mu\text{m}^2$  in the  $ac$  plane and 1 mm along the  $b$  axis.

## IV. MAGNETIZATION MEASUREMENTS

The magnetic susceptibility  $\chi$  as a function of temperature is shown in Fig. 2(a) on a single crystal of  $1 \pm 0.1$  mg. The susceptibility increases monotonically with decreasing temperature, following a modified Curie-Weiss law. Fitting our data to this law between  $T = 150$  and 300 K yields an effective moment  $\mu_{\text{eff}} \approx 4.4\mu_B/\text{Yb}$  and Curie-Weiss temperature  $T_{\text{CW}}$  ranging from  $-5$  to  $-21$  K depending on the field orientation. A large effective moment that is close to the free  $\text{Yb}^{3+}$  ion magnetic moment of  $4.54\mu_B$  indicates that the magnetic moment mainly originates from the Yb atoms while the contribution from Fe atoms is negligible. Studies of the isostructural compounds  $R\text{Fe}_5\text{P}_3$  ( $R = \text{Gd}, \text{Ho}, \text{Er}, \text{Tm}$ ) also find the Fe atoms to be nonmagnetic [23,24]. No magnetic ordering is observed down to  $T = 2$  K in  $\text{YbFe}_5\text{P}_3$ , but the enhanced susceptibility at low temperatures implies that the system might be close to a magnetic instability. The magnetization at 2 K as a function of magnetic field with different field orientations is shown in Fig. 2(b). There is a mild magnetic anisotropy  $\chi_a/\chi_{b,c}$  of  $\sim 2$  at  $T = 2$  K. The data indicate that the  $a$  axis is the easy axis.

## V. TRANSPORT PROPERTIES

The temperature dependence of resistivity along the chain direction,  $\rho_{yy}(T)$ , is shown in Fig. 3(a) for  $\text{YbFe}_5\text{P}_3$  and  $\text{LuFe}_5\text{P}_3$ . The low residual resistivity of the Yb analog of less than  $2 \mu\Omega \text{ cm}$ , combined with a high RRR of more than 60, indicates the high quality of the sample and a long mean free path at low temperatures. A magnetic field of  $B = 0.2$  T was applied to suppress a partial superconducting transition at 3.7 K. This transition is not observed in the heat capacity data shown below, and hence we attribute it to an impurity phase most likely from the Sn flux. The resistivity decreases

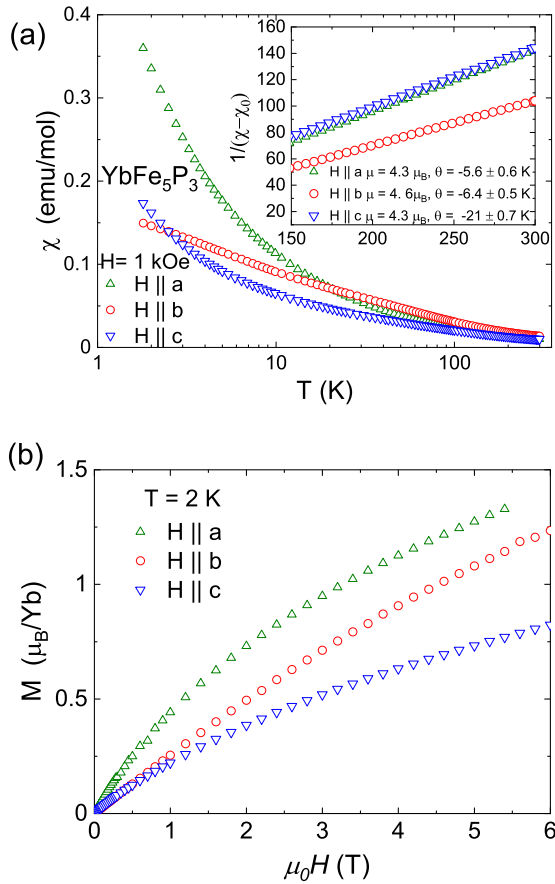


FIG. 2. (a) Magnetic susceptibility  $\chi$  as a function of temperature for field along the  $a$  (green up-pointing triangles),  $b$  (red circles), and  $c$  axes (blue down-pointing triangles). Inset: The modified Curie-Weiss plot  $1/(\chi - \chi_0)$ , where  $\chi_0 = 0.0029$ ,  $0.0039$ , and  $0.0029$  emu/mol for  $H \parallel a$ ,  $b$ , and  $c$ , respectively. The magnetic moment and Curie-Weiss temperatures from the fits to the modified Curie-Weiss law are reported in the inset. (b) Magnetic field dependence of magnetization with  $H \parallel a$  (green up-pointing triangles),  $H \parallel b$  (red circles), and  $H \parallel c$  (blue down-pointing triangles). The data were taken at  $T = 2$  K.

almost linearly from room temperature. At 25 K  $\rho(T)$  has a weak inflection point, which may reflect the presence of low-lying crystal field levels or the onset of a lattice coherence scale  $T^*$ . Below 5 K the resistivity begins to drop again, and at roughly 0.5 K the resistivity rolls over from a quasilinear temperature dependence at higher  $T$  towards a  $T^2$  Fermi-liquid-like behavior at low temperatures. The coefficient of the  $T^2$  dependence is  $2.8 \mu\Omega \text{ cm}/\text{K}^2$ . There are no anomalies reflective of long-range order in the electrical transport of YbFe<sub>5</sub>P<sub>3</sub> down to  $T = 0.12$  K.

The temperature dependence of the Hall resistivity,  $\rho_{xy}(T)$ , at  $H = 2$  T is shown in Fig. 3(b).  $\rho_{xy}$  is linear with field up to  $H = 2$  T over the measured temperature range from 2 to 50 K.  $\rho_{xy}(T)$  gradually increases with decreasing temperature, as is common in many heavy-fermion materials in the high-temperature limit [25]. The peak in  $\rho_{xy}$  at  $T = 12$  K may reflect the system entering into a lattice coherent state. The peak temperature can be smaller than that of the coherence temperature depending on the properties of the heavy fluid

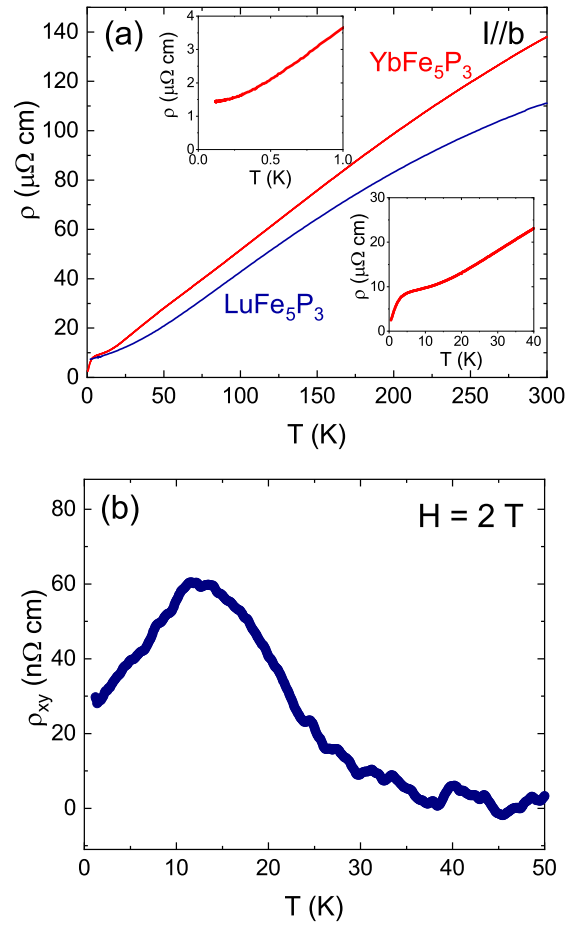


FIG. 3. (a) The temperature dependence of resistivity along the chain direction. A magnetic field of  $H = 0.2$  T was applied to suppress the superconductivity from an impurity. Insets: The expanded data between  $T = 0$  and 40 K (lower right) and between 0 and 1 K (upper left). (c) Transverse resistivity  $\rho_{xy}$  versus temperature. A magnetic field of  $H = \pm 2$  T was applied perpendicular to the chain direction and the data are antisymmetrized.

[26]. At 2 K,  $\rho_{xy}$  begins showing nonlinearity above 2 T and up to 9 T, reflecting the multiband nature of the electronic structure (not shown).

## VI. SPECIFIC HEAT

The specific heat divided by temperature,  $C_p/T$ , as a function of temperature is shown in Fig. 4. For YbFe<sub>5</sub>P<sub>3</sub> and LuFe<sub>5</sub>P<sub>3</sub>, collections of several single crystals with a total mass of 0.66 and 0.8 mg were measured, respectively. The Lu analog has the behavior of a typical metal, although the Sommerfeld coefficient  $\gamma = 110$  mJ/mol K<sup>2</sup> is enhanced relative to most metals. This enhanced Sommerfeld coefficient suggests that even if the Fe atoms do not carry a magnetic moment, they provide electronic correlations that lead to a moderate mass enhancement in the system. The low-temperature heat capacity of YbFe<sub>5</sub>P<sub>3</sub> shows a dramatic enhancement relative to the Lu analog.  $C_p/T$  increases monotonically with decreasing temperature below 10 K to approximately 0.5 K. At 0.5 K there is a tendency towards saturation, which likely reflects the crossover toward Fermi-

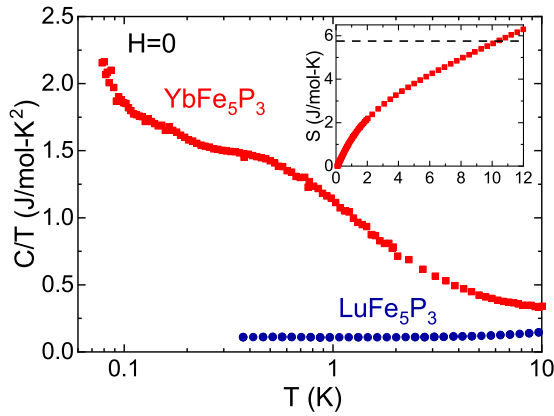


FIG. 4. Specific heat divided by temperature,  $C/T$ , as a function of temperature at low temperatures for  $\text{YbFe}_5\text{P}_3$  (red squares) and  $\text{LuFe}_5\text{P}_3$  (blue circles). An upturn below  $T = 0.2$  K originates from the nuclear Schottky anomaly. Inset: Entropy of  $\text{YbFe}_5\text{P}_3$  versus temperature. The dashed line shows  $R \ln 2 = 5.76$  J/mol K.

liquid behavior with a Sommerfeld coefficient  $\sim 1.5$  J/mol  $\text{K}^2$ . This is consistent with the crossover from quasilinear to  $T^2$  temperature dependence observed in the resistivity at 0.5 K. The comparison of the Sommerfeld coefficient with  $T^2$  resistivity gives a Kadowaki-Woods ratio  $A/\gamma^2 = 1.2 \times 10^{-6} \mu\Omega \text{ cm}/(\text{mJ}/\text{mol K}^2)^2$ . The upturn below  $T \sim 0.2$  K is consistent with a nuclear Schottky anomaly, which increases with increasing magnetic field according to the functional form  $C_{\text{nuc}} = (\alpha + \beta H^2)/T^2$  with  $\alpha = 0.421$  mJ K/mol and  $\beta = 0.027$  mJ K/mol  $\text{T}^2$ . No magnetic ordering or superconductivity was observed down to 0.1 K. The calculated entropy  $S$  is shown in the inset of Fig. 4.  $S$  reaches  $\frac{1}{2}R \ln 2$  by 3 K and  $R \ln 2$  by 10 K, which implies that the Yb ions are in a doublet ground state in the crystalline electric field. The small characteristic energy scale of a few kelvin further suggests a close proximity of the system to a quantum critical point.

## VII. THEORETICAL CALCULATIONS

Shown in Fig. 5 are the Fermi surfaces obtained by the DFT calculations. Because the nature of the  $f$  electron is currently unknown, both itinerant [Fig. 5(a)] and localized [Fig. 5(b)]

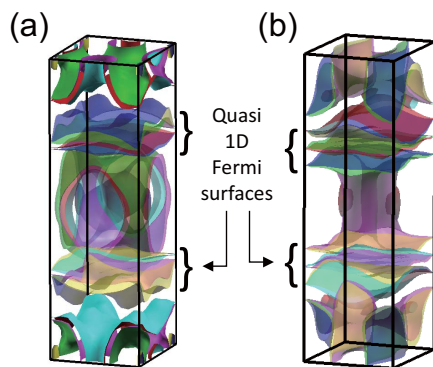


FIG. 5. DFT computed Fermi surfaces of  $\text{YbFe}_5\text{P}_3$  for (a) the itinerant configuration and (b) the localized configuration of the  $f$  electron. Different colors are used to simply distinguish different Fermi surface sheets.

configurations are plotted. To localize the  $f$  electron it was treated as a core electron in the calculation. In both configurations, many Fermi surface sheets can be seen, which is a consequence of the nine unique atomic sites in the crystal structure together with four formula units per unit cell. Band touching points along various edges of the Brillouin zone are enforced by the glide and screw symmetries that exist in this space group. The Fermi surface plots illustrate that several 1D-like Fermi surfaces are observed in addition to three-dimensional (3D) Fermi pockets, as expected from the crystal structure. The quasi-1D Fermi surface sheets can be identified as flat sheets, due to the lack of dispersion in the  $k_x$  and  $k_z$  directions. The finite amount of warping reflects that the dispersion is not perfectly 1D. Given the large RRR, quantum oscillation studies would be interesting to distinguish whether the localized or itinerant electronic structure is correct.

## VIII. MAGNETIC FIELD DEPENDENCE

The magnetic field dependence of specific heat after subtraction of the nuclear Schottky contribution  $C_{\text{nuc}}$  with field applied along the chain direction is shown in Fig. 6(a). With increasing magnetic field,  $(C - C_{\text{nuc}})/T$  is monotonically suppressed. In addition, the temperature range over which a constant  $(C - C_{\text{nuc}})/T$  behavior is observed increases with increasing magnetic field. This behavior indicates that the quantum fluctuations, which renormalize the electronic structure, are suppressed with the application of a magnetic field, and an increasingly robust Fermi-liquid state is recovered.

Very similar behavior is observed in a second sample measured down to 0.4 K with magnetic fields perpendicular to the chain direction ( $H \parallel c$ ) as shown in Fig. 6(b). The similar behavior between the two orthogonal field directions is consistent with the weak magnetic anisotropy observed in the magnetization measurements. A second resistivity sample was also measured as a function of temperature with increasing magnetic fields for  $H \parallel c$  as shown in Fig. 6(c). In zero field,  $\rho$  shows a shoulder at around 2 K, below which  $\rho$  decreases almost linearly as  $T$  decreases, consistent with non-Fermi-liquid behavior associated with strong quantum fluctuations. From the data in Fig. 3 we know that the crossover to Fermi-liquid behavior occurs below 0.5 K. When a magnetic field is applied, however, the low-temperature resistivity curves have a parabolic behavior to much higher temperatures, indicating the enhancement of the Fermi-liquid state. As indicated by arrows, the resistivity starts to deviate from a parabolic fit at higher temperatures with higher fields, and the  $T^2$  coefficient is suppressed at 8 T relative to 5 T. These facts also suggest the Fermi-liquid behavior becomes more robust with larger applied magnetic fields. The calculated Kadowaki-Woods ratio is  $1.5 \times 10^{-6} \mu\Omega \text{ cm}/(\text{mJ}/\text{mol K}^2)^2$  for both 5 and 8 T. This value is similar to the zero-field value and is typical of Yb-based heavy-fermion systems [27].

## IX. PRESSURE DEPENDENCE

The results above suggest that the system may be close to a quantum critical point at ambient pressure. The application of pressure pushes the valence state of Yb from  $2+$  towards  $3+$  and thereby favors magnetism. This motivates us to apply

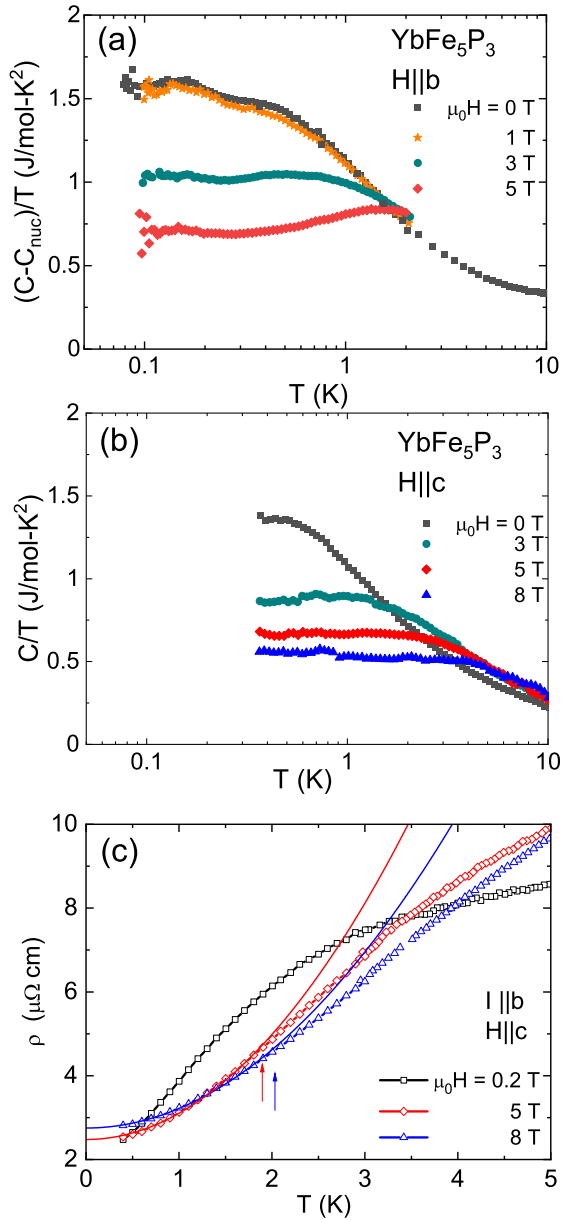


FIG. 6. (a) Specific heat divided by temperature,  $C/T$ , versus temperature at different magnetic fields applied parallel to the  $b$  axis. The nuclear Schottky contribution  $C_{\text{nuc}}$  has been subtracted from the data as described in the text. (b)  $C/T$  at different magnetic fields applied parallel to the  $c$  axis. (c) Resistivity  $\rho$  versus temperature at different magnetic fields applied parallel to the  $c$  axis showing the suppression of the non-Fermi-liquid behavior with fields. The solid lines are quadratic fits to the form  $\rho(T) = \rho_0 + AT^2$  between the base temperature and 1.5 K.  $A$  is 0.626 and 0.467  $\mu\Omega$  cm/K<sup>2</sup> for 5 and 8 T, respectively. Arrows indicate the position where the resistivity starts to deviate from the quadratic curves.

pressure to  $\text{YbFe}_5\text{P}_3$  with the goal of finding a magnetic instability. The pressure dependence of  $\rho$  as a function of temperature is shown in Fig. 7. At temperatures above 2 K, the resistivity change induced by pressure is subtle. The inflection point near 25 K shifts slightly to higher temperature. Below  $T = 2$  K, however, the inelastic scattering observed in the resistivity is pushed to lower temperatures with increasing

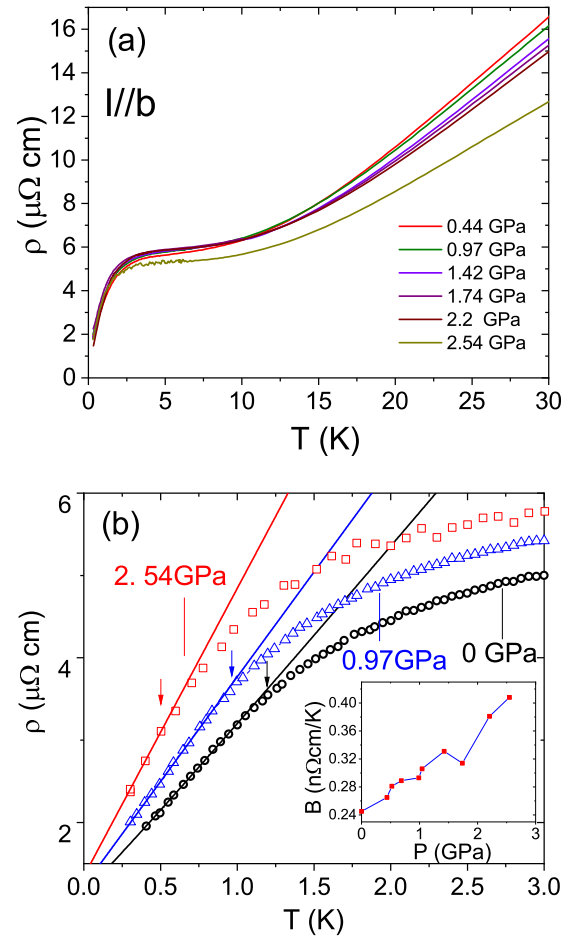


FIG. 7. (a) The pressure dependence of resistivity  $\rho$  versus temperature from  $P = 0$  to 2.2 GPa. (b) An expanded view of the pressure-dependent resistivity data between  $T = 0$  and 3 K for selected pressures 0 (black circles), 0.97 (blue triangles), and 2.54 (red squares) GPa. Solid lines are linear fits to  $\rho(T) = \rho_0 + BT$  at low temperatures. Arrows indicate where  $\rho$  deviates from the linear behavior. Inset: The slope of the linear fitting parameter  $B$  as a function of pressure.

pressure suggesting the enhancement of quantum fluctuations. Likely because the data do not go to low enough temperatures, it is difficult to quantify the enhancement of inelastic scattering. Nevertheless, in an attempt to do so, we take the linear slope of the resistivity in the low-temperature limit. We note that although  $T$ -linear behavior is often associated with non-Fermi-liquid behavior at a quantum critical point, we do not claim this is an intrinsic property of  $\text{YbFe}_5\text{P}_3$  due to the limited temperature range over which we observe this behavior. The pressure dependence of the slope is shown in the inset of Fig. 7(b). The enhanced slope with increasing pressure suggests that the system is being driven closer to a quantum critical point. We also note that the temperature at which the resistivity deviates from  $T$ -linear behavior shrinks with increasing pressure, as indicated by the arrows shown in Fig. 7(b). It would be interesting to apply even higher pressures, and possibly lower temperature measurements, to see if a quantum phase transition and/or magnetic order could be stabilized.

## X. DISCUSSION

The low-temperature ( $\lesssim 5$  K) resistivity and heat capacity reveal the presence of strong quantum fluctuations without long-range order down to 80 mK in  $\text{YbFe}_5\text{P}_3$ , with an apparent crossover towards Fermi-liquid behavior below  $\sim 0.5$  K. This type of behavior is commonly found in Ce- and Yb-based intermetallics where the competition between the Kondo and RKKY interactions leads to a QCP between magnetically ordered and disordered states [1–4]. In this scenario,  $\text{YbFe}_5\text{P}_3$  lies just past the QCP on the magnetically disordered side. It is thus surprising that magnetic order could not be found upon the application of 2.5 GPa of pressure. An alternative picture is that the strong quantum fluctuations arise because of the reduced dimensionality of the system. A truly one-dimensional magnetic system cannot possess magnetic order at finite temperature [28]. The structural aspect of the Yb chains coupled with some quasi-1D Fermi surface sheets may lead to strongly one-dimensional magnetic interactions. In this view, the lack of magnetic ordering is natural, even if the Yb ions were highly localized, and no amount of pressure could lead to magnetic order. In reality, the crossover towards Fermi-liquid behavior would not be expected in a purely one-dimensional system. We posit, however, that the extended pressure regime of strong quantum fluctuations may be enhanced by the reduced dimensionality of the system.

Further neutron and NMR work would be useful to investigate the magnetic dimensionality in this system.

In summary, we have investigated the low-temperature transport and thermodynamic properties of  $\text{YbFe}_5\text{P}_3$ . Magnetization and transport data reveal a high energy scale, which varies between 10 and 30 K depending on the measurement. This likely reflects either the influence of excited crystal field levels, a lattice coherence temperature, or a combination of the two. Below 5 K, strong quantum fluctuations lead to a strongly enhanced heat capacity and a strong downturn in the resistivity. These quantum fluctuations are either suppressed by a magnetic field, or enhanced by the application of pressure. Given the high purity of  $\text{YbFe}_5\text{P}_3$  single crystals, we believe that this is an interesting system to further explore the interplay of reduced dimensionality and quantum criticality in heavy fermions as may also be explored in  $\text{YbNi}_4\text{P}_2$  and  $\text{CeRh}_6\text{Ge}_4$ , among others.

## ACKNOWLEDGMENTS

This work was carried out under the auspices of the U.S. Department of Energy, Office of Science, Basic Energy Sciences, Materials Sciences and Engineering Division. T.A. acknowledges support of the LANL LDRD program. Pressure measurements were performed with support from the LANL LDRD program.

- 
- [1] N. Mathur, F. Grosche, S. Julian, I. Walker, D. Freye, R. Haselwimmer, and G. Lonzarich, *Nature (London)* **394**, 39 (1998).
- [2] P. Gegenwart, Q. Si, and F. Steglich, *Nat. Phys.* **4**, 186 (2008).
- [3] P. Coleman and A. J. Schofield, *Nature (London)* **433**, 226 (2005).
- [4] H. von Löhneysen, A. Rosch, M. Vojta, and P. Wölfle, *Rev. Mod. Phys.* **79**, 1015 (2007).
- [5] S. Doniach, *Physica B+C (Amsterdam)* **91**, 231 (1977).
- [6] Q. Si, *Phys. B: Condens. Matter* **378**, 23 (2006).
- [7] Q. Si, *Phys. Status Solidi B* **247**, 476 (2010).
- [8] P. Coleman and A. H. Nevidomskyy, *J. Low Temp. Phys.* **161**, 182 (2010).
- [9] S. Friedemann, T. Westerkamp, M. Brando, N. Oeschler, S. Wirth, P. Gegenwart, C. Krellner, C. Geibel, and F. Steglich, *Nat. Phys.* **5**, 465 (2009).
- [10] E. D. Mun, S. L. Bud'ko, C. Martin, H. Kim, M. A. Tanatar, J.-H. Park, T. Murphy, G. M. Schmiedeshoff, N. Dilley, R. Prozorov, and P. C. Canfield, *Phys. Rev. B* **87**, 075120 (2013).
- [11] T. Tomita, K. Kuga, Y. Uwatoko, P. Coleman, and S. Nakatsuji, *Science* **349**, 506 (2015).
- [12] H. Zhao, J. Zhang, M. Lyu, S. Bachus, Y. Tokiwa, P. Gegenwart, S. Zhang, J. Cheng, Y.-f. Yang, G. Chen, Y. Isikawa, Q. Si, F. Steglich, and P. Sun, *Nat. Phys.* **15**, 1261 (2019).
- [13] C. Krellner, S. Lausberg, A. Steppke, M. Brando, L. Pedrero, H. Pfau, S. Tencé, H. Rosner, F. Steglich, and C. Geibel, *New J. Phys.* **13**, 103014 (2011).
- [14] A. Steppke, R. KÜchler, S. Lausberg, E. Lengyel, L. Steinke, R. Borth, T. Lühmann, C. Krellner, M. Nicklas, C. Geibel *et al.*, *Science* **339**, 933 (2013).
- [15] E. Matsuoka, C. Hondo, T. Fujii, A. Oshima, H. Sugawara, T. Sakurai, H. Ohta, F. Kneidinger, L. Salamakha, H. Michor *et al.*, *J. Phys. Soc. Jpn.* **84**, 073704 (2015).
- [16] B. Shen, Y. Zhang, Y. Komijani, M. Nicklas, R. Borth, A. Wang, Y. Chen, Z. Nie, R. Li, X. Lu *et al.*, *Nature (London)* **579**, 51 (2020).
- [17] L. Wu, W. Gannon, I. Zaliznyak, A. Tsvelik, M. Brockmann, J.-S. Caux, M. Kim, Y. Qiu, J. Copley, G. Ehlers *et al.*, *Science* **352**, 1206 (2016).
- [18] R. E. Baumbach, J. J. Hamlin, L. Shu, D. A. Zocco, J. R. O'Brien, P.-C. Ho, and M. B. Maple, *Phys. Rev. Lett.* **105**, 106403 (2010).
- [19] R. E. Baumbach, J. J. Hamlin, M. Janoschek, J. Singleton, and M. B. Maple, *J. Phys.: Condens. Matter* **28**, 046004 (2016).
- [20] J. P. Perdew, K. Burke, and M. Ernzerhof, *Phys. Rev. Lett.* **77**, 3865 (1996).
- [21] P. Blaha, *et al.* WIEN2K: An Augmented Plane Wave + Local Orbitals Program for Calculating Crystal Properties (Technische Universität Wien, Wien, Austria, 2001).
- [22] W. Jeitschko, U. Meisen, and U. Scholz, *J. Solid State Chem.* **55**, 331 (1984).
- [23] H. Raffius, E. Mörsen, B. Mosel, W. Müller-Warmuth, T. Hilbich, M. Reehuis, T. Vomhof, and W. Jeitschko, *J. Phys. Chem. Solids* **52**, 787 (1991).
- [24] C. M. Thompson, Ph.D. thesis, Florida State University, 2012.
- [25] A. Fert and P. M. Levy, *Phys. Rev. B* **36**, 1907 (1987).
- [26] Y.-f. Yang, *Rep. Prog. Phys.* **79**, 074501 (2016).
- [27] N. Tsujii, H. Kontani, and K. Yoshimura, *Phys. Rev. Lett.* **94**, 057201 (2005).
- [28] R. J. Birgeneau and G. Shirane, *Phys. Today* **31**, 32 (1978).